ACS Catalysis

Research Article

pubs.acs.org/acscatalysis

Well-Defined Surface Species [(≡Si—O—)W(═O)Me_3] Prepared by Direct Methylation of [(≡Si—O—)W(═O)Cl_3], a Catalyst for Cycloalkane Metathesis and Transformation of Ethylene to Propylene†

Ali Hamieh, Yin Chen, Safwat Abdel-Azeim, Edy Abou-hamad, Serena Goh, Manoja Samantaray, Raju Dey, Luigi Cavallo, and Jean Marie Basset*

Physical Sciences and Engineering, KAUST Catalysis Center, King Abdullah University of Science and Technology (KAUST), Thuwal 23955-6900, Saudi Arabia

Supporting Information

ABSTRACT: The silica-supported tungsten oxo-trimethyl complex [(≡Si—O—)W(═O)Me_3] was synthesized using a novel SOMC synthetic approach. By grafting the inexpensive stable compound $WOCl_4$ on the surface of silica, partially dehydroxylated at 700 °C ($SiO_{2\text{-}700}$), a well-defined monopodal surface complex [(≡Si—O—)W(═O)Cl_3] was produced. The supported complex directly methylated with $ZnMe_2$ and transformed into [(≡Si—O—)W(═O)Me_3], which we fully characterized by microanalysis, IR, mass balance and SS NMR (^{1}H, ^{13}C, ^{1}H−^{13}C HETCOR, ^{1}H−^{1}H DQ and TQ). [(≡Si—O)W(═O)Me_3] has two conformational isomers on the surface at room temperature. The conversion of one to the other was observed at 318 K by variable-temperature ^{13}C CP/MAS and ^{1}H spin echo MAS solid-state NMR; this was also confirmed by NMR and DFT calculations. [(≡Si—O)W(═O)Me_3] was found to be active in cyclooctane metathesis and to have a wide distribution range in ring-contracted and ring-expanded products. In addition, [(≡Si—O)W(═O)Me_3] proved to be highly active for selective transformation of ethylene to propylene compared to other silica-supported organometallic complexes.

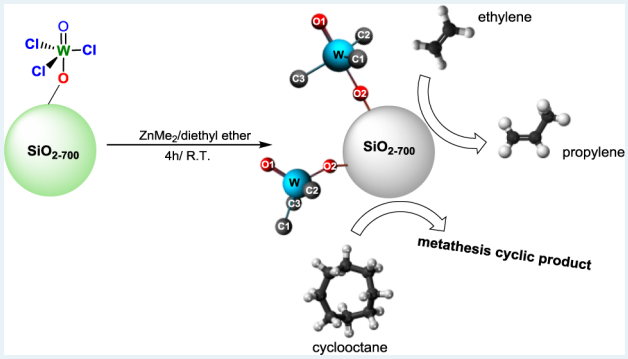

KEYWORDS: *surface organometallic chemistry, tungsten oxo compound, surface methylation, cyclooctane metathesis, ethylene propylene conversion*

INTRODUCTION

Current environmental challenges regarding green chemistry,[1] sustainability,[2] and energy requirements[3] demand that the chemical industry develop more active and more selective catalytic reactions.[4] This is not always possible with classical heterogeneous catalysts, which are not always well-defined. The highest possible selectivity and activity require well-defined heterogeneous catalysts.[5] These well-defined catalysts must have the greatest possible number of active sites with uniform composition. In addition, if their lifetime is limited, they must be regenerable and easily prepared.

Single-site catalysts offer a possible solution to these problems. One of the best ways to achieve control of catalyst structure at the atomic and molecular level (catalysis by design strategy) is to carefully graft organometallic complexes (or coordination compounds) directly onto solid surfaces (oxides, porous materials, or sometimes metallic nanoparticles), using the concepts and tools of surface organometallic chemistry (SOMC).[6] Many new catalytic reactions have been discovered using this strategy including Ziegler−Natta depolymerization[7] and alkane metathesis.[8] Often these reactions involving C−H and C−C bond activation and cleavage were discovered with oxide-supported transition metal hydrides (e.g., M = Ti,[9] Zr,[10] Hf,[11] Ta,[12] W[13]) in which the metal hydride is linked to the oxide surface one-by-one or via many O−M bonds.

Although the synthesis of well-defined surface organometallic complexes provides a better understanding in terms of the reaction mechanism and determining the first elementary step, these materials are still far from commercialization because of their high cost and complexity in synthesis.

Recently, when working with Ta and W, we found that starting with a metal methyl rather than a metal hydride may open up a pathway to simpler synthetic steps.[14] Here we report a general process for the synthesis of a single-site well-defined catalyst using a simpler and more economical method than previously proposed. The concept is to graft by means of

Received: December 23, 2014
Revised: February 17, 2015
Published: February 18, 2015

ACS Publications © 2015 American Chemical Society

DOI: 10.1021/cs5020749
ACS Catal. 2015, 5, 2164−2171

metal–halide coordination compounds rather than metal–alkyls organometallic complexes. For example, using previous methods we successfully grafted transition metal halides onto silica (e.g., dodecacarbonyl-trihydroiodo-tetraosmiun).[15]

In this work, inspired by the reactivity of surface metal–methyl complexes,[14,16−19] we developed a new strategy to simplify the synthesis of surface organometallic compounds and best maintain their well-defined character throughout post-grafting synthesis. The new strategy is composed of two main steps: grafting inexpensive commercially available metal halides and then selectively alkylating (methylate) the grafted complexes to form catalytically active metal–CH_3 groups.

Here we describe a simple method for the synthesis of a novel silica-supported tungsten oxo-trimethyl complex [(≡Si—O—)W(=O)Me_3]. Our synthesis protocol follows a sequence of grafting the commercially available tungsten(VI) oxy-tetrachloride on silica, dehydroxylated at 700 °C ($SiO_{2\text{-}700}$) under high vacuum, followed by alkylation of the grafted complex. A similar strategy was recently published,[20] however, using $SiO_{2\text{-}200}$ to produce a bipodal species that is different [(≡Si—O)$_2$W(=O)Me_2].[20] We fully characterized the silica-supported tungsten oxo-trimethyl using solid-state NMR, FT-IR spectroscopy, microanalysis, and mass balance and validated it by NMR-DFT calculations. The new tungsten oxo-trimethyl catalyst showed significant activity in various organic transformations, especially in cyclooctane metathesis and direct transformation of ethylene to propylene.

■ RESULTS AND DISCUSSION

Preparation and Characterization of [(≡Si—O—)W(=O)Me_3] on $SiO_{2\text{-}700}$. [(≡Si—O—)W(=O)Cl_3] (**2**) was used as the precursor for the synthesis of **3**. Surface compound **2** was prepared by grafting $WOCl_4$ on silica Aerosil 200 partially dehydroxylated overnight under 10^{-5} bar at 700 °C ($SiO_{2\text{-}700}$) (Scheme 1). The reaction was performed in

Scheme 1. Synthesis of [(≡Si—O—)W(=O)Cl_3] (2) by Reaction of 1 with Partially Dehydroxylated Silica at 700 °C ($SiO_{2\text{-}700}$)

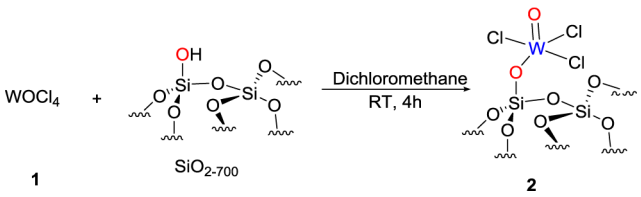

dichloromethane at room temperature for 4 h. A partial vacuum was used to prevent any secondary reactions by gaseous hydrogen chloride liberated during the reaction with the support. Excess physisorbed molecular complexes were removed by washing the solid three times with dichloromethane (3 × 20 mL). The resulting light green material was dried under high vacuum (10^{-5} bar) pressure. The infrared spectrum showed that the characteristic peak of free silanol at 3743 cm^{-1} (Figure 1A) completely disappeared (Figure 1B). The elemental analysis of the light green powder (product **2**) found 4.84% W and 2.59% Cl with a ratio of W/Cl = 1.0/2.7 ± 0.2 (theoretical ratio for monopodal 1.0/3.0).

Mass balance determination was performed on [(≡Si—O—)W(=O)Cl_3] by hydrolysis with water; measurement of the amount of released hydrogen chloride was performed using silver nitrate. A ratio of 2.8 ± 0.2 chlorides per grafted tungsten

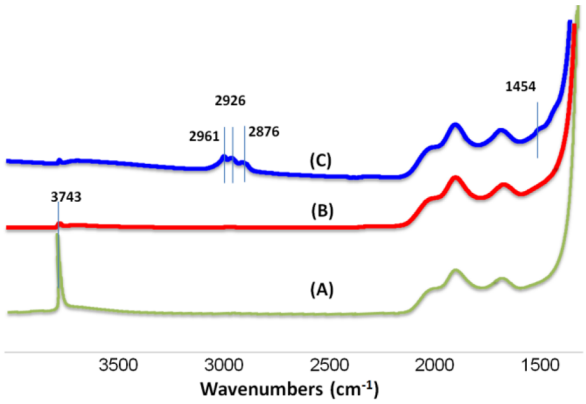

Figure 1. (A) SiO_{2-700}; (B) after grafting of $WOCl_4$; (C) after alkylation with $ZnMe_2$.

atom was found. Mass balance and gas quantification studies confirmed that there are three chlorides per tungsten.

Direct methylation of [(≡Si—O—)W(=O)Cl_3] was achieved using various alkylating agents such as $ZnMe_2$, $SnMe_4$, MeLi, and Al_2Me_6. Partially methylated species were produced with $SnMe_4$, whereas MeLi and Al_2Me_6 caused violent reactions that formed insoluble salts. The best result was obtained after treatment of [(≡Si—O—)W(=O)Cl_3] with 1.5 equiv of $ZnMe_2$ in diethyl ether at room temperature for 4 h (Scheme 2).

Scheme 2. Synthesis of Supported [(≡Si—O—)W(=O)Me_3] (3) by Surface Methylation of 2 with 1.5 equiv of Dimethylzinc

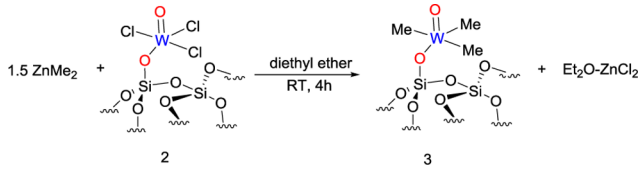

This treatment provided us high selectivity in favor of fully methylated surface complex [(≡Si—O—)W(=O)Me_3] **3**.

The IR spectrum (Figure 1C) revealed new bands in the range of 3000 cm^{-1}, ν(C–H), and 1454 cm^{-1}, δ(C–H), assigned to methyl fragments. Microanalysis associated with gas quantification results revealed the ratio of carbon to tungsten (C/W) in complex **3** (2.8 ± 0.2) (theoretical value of 3). The elemental analysis gave 4.81% W, 1.2% C, 1.01% Zn, and 1.56% Cl, with a ratio of C/W = 3.5 (theoretical value of 3) and a ratio of Cl/Zn = 2.1; these results suggest that we have about three methyl groups bonded to tungsten. Some remaining diethyl ether coordinated to zinc chloride (vide infra) accounts for the higher carbon to tungsten ratio.

NMR Study. The prepared surface complex **3*** was characterized by solid-state NMR. The ^{1}H magic-angle spinning (MAS) NMR spectrum of **3** at room temperature (Figure 2) exhibits a main signal at 1.4 ppm with a shoulder at 1.9 ppm and broad signal at 3.6 ppm. The signals at 1.4 and 1.9 ppm autocorrelate in two-dimensional (2D) double-quantum (DQ) (2.8 and 3.8 ppm in F_1) (Figure 3A) and triple-quantum (TQ) (4.2 and 5.7 ppm in F_1) (Figure 3B) spectra and are assigned to methyl groups connected to tungsten. The proton resonance at 3.6 ppm with less than an 11% intensity ratio was assigned to the CH_2 group of the coordinated ether and supported by an

DOI: 10.1021/cs5020749
ACS Catal. 2015, 5, 2164−2171

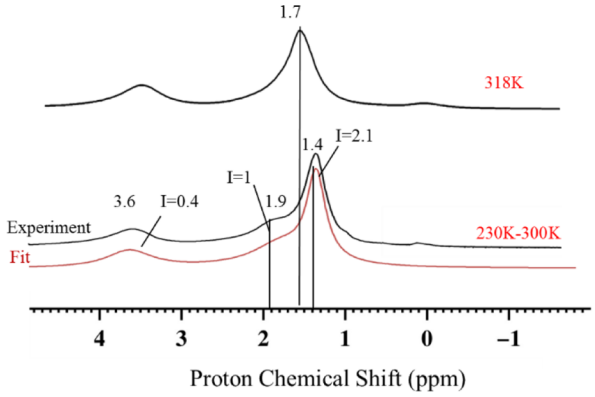

Figure 2. 1D ^{1}H MAS solid-state NMR spectra of **3*** acquired at 600 MHz at different temperatures with a 22 kHz MAS frequency and a repetition delay of 5 s and 8 scans.

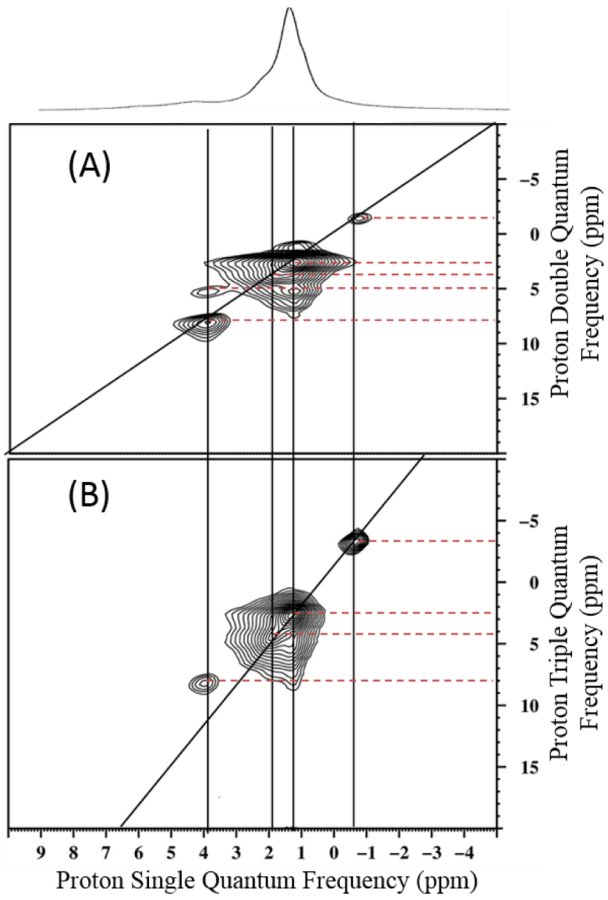

Figure 3. (A) 2D ^{1}H−^{1}H DQ/SQ and (B) ^{1}H−^{1}H TQ/SQ NMR spectra of **3*** at room temperature (both acquired with number of scans per increment = 32 per t_1 increment, repetition delay = 5 s, number of individual t_1 increments = 128).

autocorrelation in the DQ (7.2 ppm in F_1) (Figure 3A) but not in the TQ spectra (Figure 3B). Furthermore, a correlation between the CH_3 and CH_2 groups of the coordinated ether was observed in both DQ and TQ NMR experiments (Figure 3). In addition, a small autocorrelation for a proton signal at −0.7 ppm in both DQ and TQ spectra indicates the presence of trace amounts of remaining dimethylzinc (<2%). To obtain a better ^{13}C MAS NMR resolution, an enriched ^{13}C carbon $Zn^*(Me)_2$ was prepared and used in synthesizing complex **3*** (^{13}C 97% enriched). The ^{13}C CP/MAS NMR spectrum (Figure 4) at room temperature of **3*** displays a main signal at 46 ppm

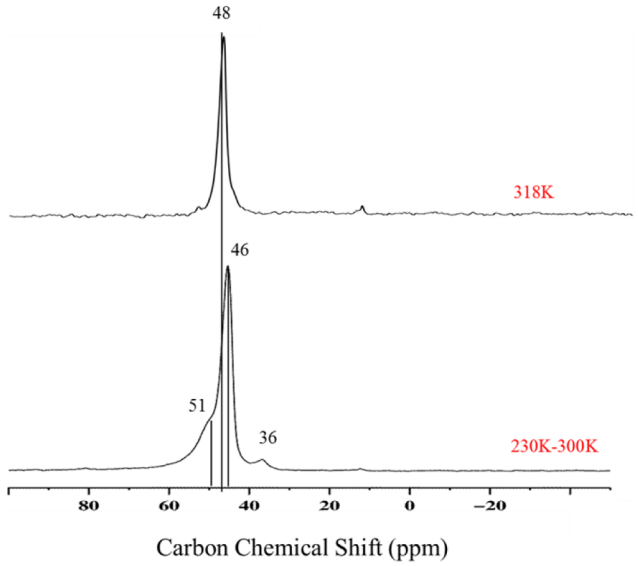

Figure 4. One-dimensional ^{13}C CP/MAS NMR spectra of **3*** at different temperatures with a 10 kHz MAS frequency (repetition delay = 5 s, contact time = 2 ms, line broadening = 80 Hz, and number of scans = 10000).

with a shoulder at 51 ppm and small peak around 36 ppm. Additionally, the 2D ^{1}H−^{13}C HETCOR NMR spectrum (Figure 5) with a short contact time (0.2 ms) shows a correlation between the methyl protons 1.4−1.9 ppm and carbon atoms 36, 46, and 51 ppm, which allows their assignment to methyl groups. Furthermore, small correlations between carbon atoms 15 and 66 ppm and protons 1.1 and 3.6 ppm, respectively, are assigned to CH_3 and CH_2 of coordinated diethyl ether.

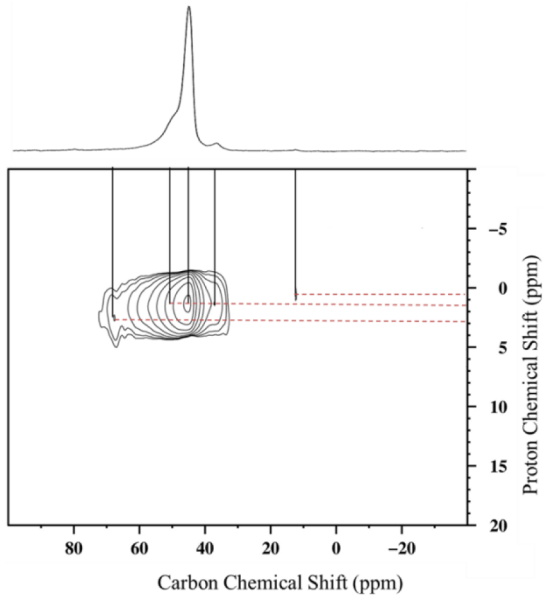

Figure 5. 2D CP/MAS HETCOR NMR spectra of **3*** acquired with short contact times of 0.2 ms under 8.5 kHz MAS frequency (number of scans per increment = 4000, repetition delay = 4 s, number of t_1 increments = 32, line broadening = 80 Hz).

DOI: 10.1021/cs5020749
ACS Catal. 2015, 5, 2164−2171

Recently, we reported that the dynamic motion of the grafted molecular complex [(≡Si—O—)WMe_5] results in the observation of a set of averaged chemical shifts.[17,21] Thus, we recorded the ^{1}H and ^{13}C solid-state NMR spectra at low and high temperatures. Figures 2 and 4 show the variable-temperature ^{1}H spin−echo MAS and ^{13}C CP/MAS solid-state NMR spectra of **3***. At 298 and 230 K the ^{1}H MAS NMR spectra show two resonances centered at 1.4 and 1.9 ppm with a 2.1:1 intensity ratio (Figure 2). The ^{13}C resonances (Figure 4) show a similar behavior with two resonances of 46 and 51 ppm observed at 298 K or lower (230 K). However, as the temperature of the sample was increased (318 K), a single resonance was observed at 1.7 and 48 ppm in the ^{1}H and ^{13}C NMR spectra, respectively (Figures 2 and 4). At 318 K, ^{1}H and ^{13}C chemical shifts are observed at the weighted average of the respective chemical shifts recorded at room and low temperatures. This suggests that the observation of a single resonance at 318 K could be a result of rapid chemical exchange between the two nonequivalent types of methyl groups, compared to the rigidity of the surface complex at room and low temperatures.

DFT NMR Calculations. We modeled tungsten species grafted on silica using the molecular model depicted in Figure 6.

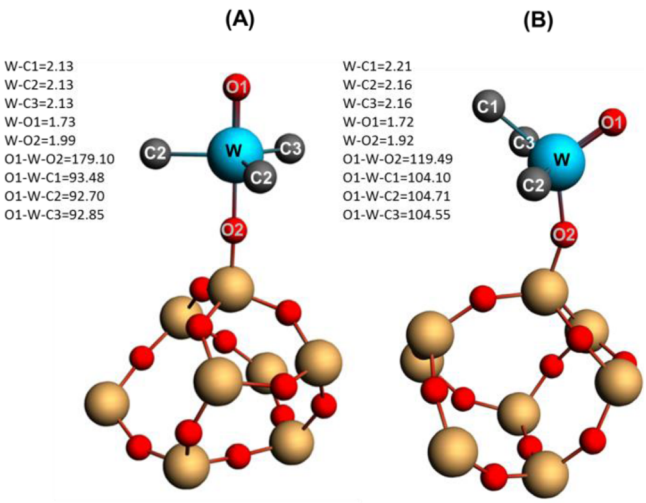

Figure 6. Ball-and-stick representations of the DFT molecular model of the −W(=O)$(Me)_3$ complex, two optimized conformations (A, B). Hydrogen atoms are omitted for clarity. Color code: W, cyan; C, gray; O, red; Si, orange. Geometric parameters are reported in angstroms for the bond distances and in degrees for angles.

We considered two conformations that differ with respect to their relative orientation of the SiO—W and W=O bonds. In the former, the oxo ligand is trans oriented to the siloxy ligand, creating a bipyramidal trigonal geometry around the metal center (Figure 6A). In the second conformation, the oxo and the siloxy ligands are cis oriented, producing an overall geometry around the metal center that is best described as a distorted square pyramid with the W=O bond at the apex (Figure 6B). According to calculations, the structure with the trans-oriented W—siloxy and W=O bonds (Figure 6A) is only 2.1 kcal/mol more stable than the structure with the same bonds cis oriented (Figure 6B). For this reason, the following DFT NMR analysis was performed on both geometries. The magnetic shielding values (^{1}H and ^{13}C) reported in Table S1 (in the Supporting Information) show a high level of agreement between the calculated and experimental carbon chemical shifts. The DFT models of the supported species indicate that the three carbons on the trigonal bipyramid model in Figure 6A possess magnetic shielding values of 142.2, 143.3, and 143.7 ppm for C1, C2, and C3, respectively. Overall, the average value of the chemical shift of these three carbons is 44.5 ppm, which is in accordance with the experimental main resonance of 46 ppm. Figure 6B illustrates a model with square pyramid geometry where C1 is predicted to be shielded by 7.8 and 8.6 ppm more than C2 and C3, respectively (Table 1). Therefore,

Table 1. DFT Calculated ^{13}C Nuclear Magnetic Shielding and Chemical Shifts for the Two Possible Geometries of Complex [(≡Si—O—)W(=O)Me_3]

methyl group	σ_{iso}(^{13}C) (ppm)	δ_{iso}(^{13}C) (ppm)	δ_{iso}(^{13}C) (ppm) av	δ_{iso}(^{13}C) (ppm) exptl
Model of Figure 6A: Trans-Oriented W=O Bonds				
C1	142.19	44.67	44.51	46
C2	143.26	43.60		
C3	143.70	43.16		
Model of Figure 6B: Cis-Oriented W=O Bonds				
C1	146.76	40.10	40.10	36
C2	138.95	47.91	48.32	51
C3	138.13	48.73		

the experimentally observed chemical shifts at 36 can be assigned to C1, whereas the 51 ppm peak is attributed to C2 and C3 (see the model of Figure 6B). Thus, the single peak at 48 ppm, 318 K, is more likely a result of a rapid isomerization between the trigonal bipyramid and the square pyramid geometries, averaging the chemical shift of carbon atoms in the different geometries.

CATALYTIC STUDY

Cyclooctane Metathesis. We predicted that complex **3** would be able to generate a tungsten methyl/methylidene surface molecule at elevated temperature (around 80 °C), which we suspected to be responsible for the metathesis reaction; therefore, we applied complex **3** for metathesis of cyclooctane. We focused on cyclooctane that can be used as a building block for higher macrocycles and is crucial in the preparation of pharmaceutical intermediates, polymers, and fragrances.[22] In a typical reaction, 400 equiv of cyclooctane was mixed with 40 mg of [(≡Si—O—)W(=O)Me_3] **3** at 150 °C in a sealed ampule for 7 days. At the end of the reaction, the ampule was frozen with liquid nitrogen, the reaction mixture was quenched with dichloromethane, and the liquid fraction was filtered and analyzed by gas chromatography. Cyclooctane was converted into cyclohexane by ring contraction (68%) and higher macrocycles by ring expansion ranging between cC_{13} and cC_{30} (30%)[23] with a turnover number (TON) of 260 as determined by GC and GC-MS (Figure 7). We know from previous results on cyclooctane metathesis that ring contraction becomes more favorable as contact time increases, knowing that the higher and lower homologues are cyclic with TON >350[23] (see Figures S2, S3, and S4 in the Supporting Information). Supplementary experiments were made, showing that the small amount of residual $ZnCl_2$ did not affect catalytic activity (SI-5).

Direct Conversion of Ethylene to Propylene. Polypropylene (PP) is becoming more and more important as a chemical for use in resolving environmental issues.[24] Therefore,

DOI: 10.1021/cs5020749
ACS Catal. 2015, 5, 2164−2171

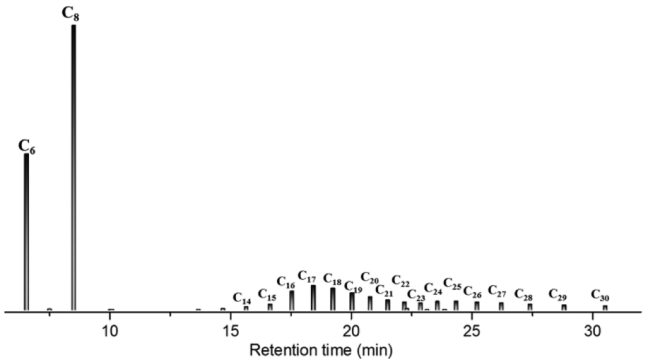

Figure 7. GC chromatogram of cyclooctane metathesis products that have been catalyzed by **3**. Reaction conditions: batch reactor, compound **3** (40 mg, 8.3 μmol; W loading, 4.83 wt %), cyclooctane (0.5 mL, 3.7 mmol), 160 h, 150 °C. Conversion = 60%, TON = 260. Products formed are ring-contracted (cC_6) as well as ring-expanded species ranging from cC_{13} to cC_{29}.

there is a high demand by industry for propylene manufacture. More than 80 million tons is produced each year worldwide; this production is going to increase in the next 10 years to reach 130 million tons annually.[25] The main source of this highly valuable building block in polymer chemistry is the steam or catalytic cracking of natural gas and oil;[26] however, these processes require large amounts of energy. In this work we found that [(≡Si—O—)W(=O)Me_3] can directly convert ethylene into propylene under milder reaction conditions than previously documented. In an earlier study, we used tungsten hydride on alumina to demonstrate that a hydride catalyst could perform ethylene dimerization to 1-butene via the metal hydride, isomerization of 1-butene to 2-butene, and cross metathesis between ethylene and 2-butene via a metallo-carbene.[27]

Our more recent research documented here is likely following the same process, but via a different initiation step. Tungsten−methyl could insert an ethylene to give tungsten−*n*-propyl, followed by a β-hydride elimination, which would generate propylene and a tungsten hydride that is necessary to propagate the dimerization of ethylene and the isomerization of the 1-butene (Scheme3). Cross metathesis could be achieved with an equilibrium between W—CH_3 and W(H)(=CH_2), which would be sufficient to promote the full catalytic cycle. We introduced ethylene (11.65 mmol) to a 300 mL glass reactor loaded with 100 mg of [(≡Si—O—)W(=O)Me_3] to produce selectively propylene after 18 h of reaction at 150 °C. We monitored the products using GC-FID and found that propylene represents >90% of the products (Table 2). This silica-supported catalyst is more active and selective when compared to its analogue tungsten hydride or tungsten pentamethyl grafted on $SiO_{2\text{-}700}$ after 18 h of reaction at 150 °C. Supplementary experiments were made, showing that the small amount of residual $ZnCl_2$ did not affect catalytic activity (SI-5).

CONCLUSION

In this paper we reported the facile selective synthesis of monopodal [(≡Si—O—)W(=O)Me_3] by grafting commercially available $WOCl_4$ onto $SiO_{2\text{-}700}$. The resultant [(≡Si—O—)W(=O)Cl_3] was then methylated by $ZnMe_2$ in diethyl ether solution to selectively give [(≡Si—O—)W(=O)Me_3]. **3** was fully characterized by SS-NMR, IR, microanalysis, and mass balance techniques. Two different conformations of **3** were proposed depending on the relative orientation of the SiO—W and W=O bonds. Experimental and DFT calculated NMR supports these models. [(≡Si—O—)W(=O)Me_3] **3** was applied as a catalyst for metathesis of cyclooctane, demonstrating significant activity in producing a wide range of ring contracted and expanded cycloalkanes. On the other hand, the tungsten oxo-trimethyl catalyst was tested for the direct transformation of ethylene to propylene and was found to have a higher activity and selectivity compared to the analogues tungsten hydride/silica and tungsten pentamethyl/silica.

Scheme 3. Proposed Mechanism for the Direct Conversion of Ethylene to Propylene on [(≡Si—O—)W(=O)Me_3] (3)

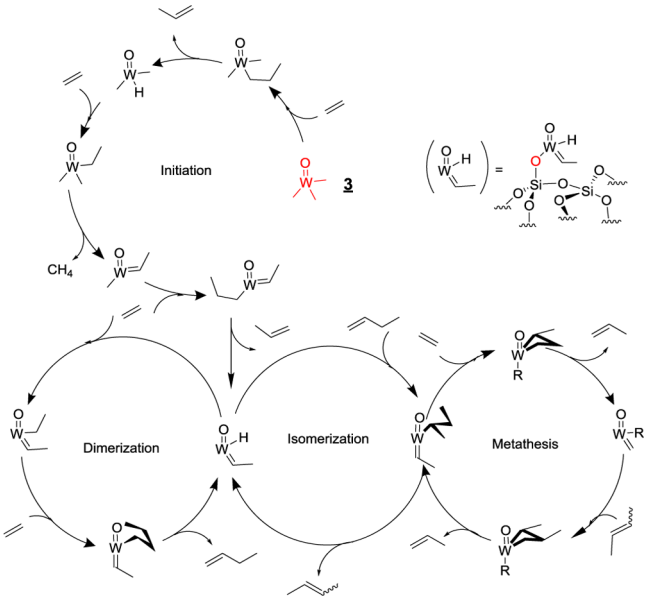

Table 2. Ethylene to Propylene Transformation Using [(≡SiO)W(=O)Me_3] As Compared to the Analogue Tungsten Hydride and Tungsten Pentamethyl

catalyst	TON[b]	product selectivity[a] (%)		
		propylene	butenes	pentenes
3	324	93.2	6.45	0.28
[≡SiO—W($Me)_5$]	75	51.6	46.3	2.01
[≡SiO—W$(H)_x$]	77	32.4	64.85	2.73

[a]The selectivity is defined as the amount of a product over the total amount of products. [b]TON is expressed in moles of ethylene transformed per mole of W.

EXPERIMENTAL SECTION

General Procedure. All experiments were performed by using standard Schlenk and glovebox techniques under an inert nitrogenous atmosphere. Syntheses and treatments of the surface species were completed using high-vacuum lines ($<10^{-5}$ mbar) and glovebox techniques. All solvents were dried, degassed, and freshly distilled prior to use according to classical methods (over CaH_2 for dichloromethane and over Na/benzophenone for diethyl ether). Ethylene was dried and deoxygenated before use by passage through a mixture of freshly regenerated molecular sieves (3 Å) and R3-15 catalysts (BASF). IR spectra were recorded on a Nicolet 6700 FT-IR spectrometer using a DRIFT cell equipped with CaF_2 windows.

DOI: 10.1021/cs5020749
ACS Catal. 2015, 5, 2164−2171

The IR samples were prepared under argon within a glovebox. Typically, 64 scans were collected for each spectrum (resolution = 4 cm^{-1}). Elemental analyses were performed at Mikroanalytisches Labor Pascher (Germany). Gas-phase analysis of alkanes was performed using an Agilent 6850 gas chromatography column with a split injector coupled with an flame ionization detector (FID). An HP-PLOT Al_2O_3 KCl 30 m × 0.53 mm, 20.00 mm, capillary column coated with a stationary phase of aluminum oxide deactivated with KCl was used with helium as the carrier gas at 32.1 kPa. Each analysis was executed under the same conditions: a flow rate of 1.5 mL/min and an isotherm at 80 °C.

Solid-State Nuclear Magnetic Resonance Spectroscopy. One-dimensional ^{1}H MAS and ^{13}C CP/MAS solid-state NMR spectra were recorded on Bruker AVANCE III spectrometers operating at 400 or 600 MHz resonance frequencies for ^{1}H. The 400 MHz experiments employed a conventional double-resonance 4 mm CP/MAS probe, whereas experiments at 600 MHz utilized a 3.2 mm HCN triple-resonance probe. In all cases the samples were packed into rotors under inert atmosphere inside gloveboxes. Dry nitrogen gas was utilized for sample spinning to prevent degradation of the samples. NMR chemical shifts are reported with respect to the external references TMS and adamantane. ^{13}C CP/MAS NMR experiments used the following sequence: 90° pulse on the proton (pulse length = 2.4 s), then a cross-polarization step with a contact time of typically 2 ms, and finally acquisition of the ^{13}C signal under high-power proton decoupling. The delay between the scans was set to 5 s to allow the complete relaxation of the ^{1}H nuclei, and the number of scans ranged between 5 000 and 10 000 for ^{13}C and was 32 for ^{1}H. An exponential apodization function corresponding to a line broadening of 80 Hz was applied prior to the Fourier transformations.

The 2D ^{1}H−^{13}C heteronuclear correlation (HETCOR) solid-state NMR spectroscopy experiments were conducted on a Bruker AVANCE III spectrometer operating at 600 MHz using a 3.2 mm MAS probe. These experiments were performed according to the following scheme: 90° proton pulse, t_1 evolution period, CP to ^{13}C, and detection of the ^{13}C magnetization under TPPM decoupling. During the cross-polarization step, a ramped radio frequency (RF) field centered at 75 kHz was applied to the protons, whereas the ^{13}C channel RF field was matched to obtain an optimal signal. A total of 32 t_1 increments with 4000 scans each were collected; sample-spinning frequency was 8.5 kHz. Using a short contact time (0.2 ms) for the CP step, the polarization transfer in the dipolar correlation experiment was verified to be selective for the first coordination sphere around tungsten, such that correlations occurred only between pairs of attached ^{1}H−^{13}C spins (C−H directly bonded).

^{1}H−^{1}H Multiple-Quantum Spectroscopy. Two-dimensional double-quantum (DQ) and triple-quantum (TQ) experiments were recorded on a Bruker AVANCE III spectrometer operating at 600 MHz with a conventional double-resonance 3.2 mm CP/MAS probe, according to the following general scheme: excitation of DQ coherences, t_1 evolution, z-filter, and detection. The spectra were recorded in a rotor-synchronized fashion in t_1 such that the t_1 increment was set equal to one rotor period (45.45 μs). One cycle of the standard back-to-back (BABA) recoupling sequences was used for the excitation and reconversion period. Quadrature detection in w_1 was achieved using the States-TPPI method. A spinning frequency of 22 kHz was used. The 90° proton pulse length was 2.5 μs, whereas a recycle delay of 5 s was used. A total of 128 t_1 increments with 32 scans per increment were recorded. The DQ frequency in the w_1 dimension corresponds to the sum of two single-quantum (SQ) frequencies of the two coupled protons and correlates in the w_2 dimension with the two corresponding proton resonances. The TQ frequency in the w_1 dimension corresponds to the sum of the three SQ frequencies of the three-coupled protons and correlates in the w_2 dimension with the three individual proton resonances. Conversely, groups of fewer than three equivalent spins will not give rise to diagonal signals in the spectrum.

Preparation of the Silica Partially Dehydroxylated at 700 °C. Typically, 4.000 g of Degussa Aerosil 200 silica was treated in a quartz reactor fitting a tubular furnace under high vacuum (10^{-5} Torr) pressure at 700 °C for 16 h. The temperature program was set to 90 °C/h. IR (cm^{-1}): 3747 (ν(SiO−H)).

Preparation of [(≡Si—O—)W(=O)Cl$_3$]. In a double Schlenk, a solution of $WOCl_4$ (342 mg, 1 mmol, 1.1 equiv with respect to the amount of surface-accessible silanols) in 25 mL of dichloromethane was allowed to react with 3.0 g of $SiO_{2\text{-}700}$ at 25 °C for 4 h. This reaction was performed under mild dynamic vacuum conditions to remove any of the HCl produced during the reaction. At the end of the reaction, the resulting light green solid was washed with dichloromethane (3 × 20 mL) and dried under a dynamic vacuum (<10^{-5} Torr, 2 h). Elemental analysis found W, 4.81%; Cl, 2.59%.

Preparation of Zn(^{13}CH$_3$)$_2$ in Ether.[17] In a 200 mL Schlenk, 15 mL of 1.6 M BuLi was taken under argon, and to that was added dropwise 3.4 g (24 mmol) of ^{13}MeI diluted in 25 mL of pentane at −20 °C with stirring. A white precipitate formed immediately, and the solution was stirred for another 30 min after the addition of ^{13}MeI. The precipitate was then filtered and dried under a vacuum to produce a white solid (^{13}MeLi). A small amount of ^{13}MeLi was taken and titrated with deoxygenated water to quantify the amount of methyl lithium present by quantifying the release of methane (around 55% ^{13}MeLi was found). In a double Schlenk, ^{13}MeLi (22 mmol, 484 mg) was added to 10 mL of diethyl ether, and to that was added a solution of anhydrous $ZnCl_2$ (10 mmol in 10 mL) at −20 °C. The reaction was allowed to reach room temperature slowly and remained at that temperature for another hour. The final product was filtered, and the dimethylzinc was collected from the filtrate.

Preparation of [(≡Si—O—)W(=O)Me$_3$]. In a double Schlenk [(≡Si—O—)W(=O)Cl]$_3$ (1.0 g, 0.3 mmol) was added to 20 mL of ether, and to that was added (0.45 mmol) $ZnMe_2$ solution in diethyl ether (1.5 equiv with respect to the amount of tungsten oxo chloride on the surface) to react at 25 °C for 4 h. At the end of the reaction, the resulting gray solid was filtered and thoroughly washed with diethyl ether. The gray solid was then dried under dynamic vacuum (<10^{-5} Torr) conditions for 4 h. ^{1}H MAS SS NMR (400 MHz, 298 K) δ 1.4 (CH_3), 1.9 (CH_3), 3.6 (CH_2); ^{13}C CP-MAS SS NMR (400 MHz, 298 K) δ 36 (CH_3), 46 (CH_3), 51 (CH_3); ^{1}H MAS SS NMR (400 MHz, 318 K) δ 1.7 (CH_3), 3.6 (CH_2); ^{13}C CP-MAS SS NMR (400 MHz, 318 K) δ 48 (CH_3). The hydrolysis of the solid with a vapor pressure of degassed water generated 0.74 ± 0.05 mmol CH_4 g^{-1} (2.8 ± 0.2 CH_4/W). Anal. Calcd 4.81% W, 1.2% C, 1.01% Zn, 1.56% Cl.

Cyclooctane Metathesis Using [(≡Si—O—)W(=O)Me$_3$]. The reactions were performed using an ampule filled with the catalyst (40 mg, 0.0083 mmol, W loading = 4.8 wt %) inside a

DOI: 10.1021/cs5020749
ACS Catal. 2015, 5, 2164−2171

glovebox where cyclooctane (0.5 mL, 3.7 mmol) was added. The ampule was sealed under vacuum pressure, immersed in an oil bath, and heated at 150 °C for 7 days. At the end of the reaction, the ampule was cooled using liquid nitrogen. The mixture was quenched by adding a fixed amount of dichloromethane after filtration; the resulting solution was analyzed by GC and GC-MS.

Ethylene to Propylene Using [(≡Si−O−)W(=O)Me$_3$]. One hundred milligrams of complex **3** was placed in a 300 mL batch reactor, and after evacuation to 10^{-5} mbar, 0.95 atm of dry ethylene was introduced (substrate/catalyst ratio around 500). The reactor was heated at 150 °C for 18 h. The final products were analyzed by GC.

DFT Computational Details. All quantum chemical computations were performed using the Amsterdam Density Functional (ADF)[28] and Gaussian 09 programs. NMR calculations were made for each of the two different conformations depicted in Figure 6. The two different models represent the position of the oxygen atoms around tungsten; in the first conformation (A) the oxygen atom is perpendicular to the plane of the three methyl groups. In the second conformation (B) the position of the oxygen atom exchanged with one methyl group.

First, geometry optimizations were performed using Gaussian 09 with the generalized gradient approximation (GGA) exchange-correlation function developed by Perdew, Burke, and Ernzerhof (PBE)[29,30] an all electron Def2_TZVP[31,32] basis set computational level. Geometry optimizations were carried out without any constraints. Optimized geometries were used as input for the ADF NMR calculations. For the magnetic shielding tensor calculations (^{1}H and ^{13}C), the zeroth-order regular approximation (ZORA)[33−35] was used to include relativistic effects of both scalar and spin−orbit contributions.[36] The NMR calculations used an all-electron triple-ζ basis set, which included two polarization functions (i.e., TZ2P) and a PBE functional.

■ ASSOCIATED CONTENT

Supporting Information

The following file is available free of charge on the ACS Publications website at DOI: 10.1021/cs5020749.

Information on optimized geometries and full disclosure of the calculated magnetic shielding values for the computational models used (PDF)

■ AUTHOR INFORMATION

Corresponding Author

*(J.M.B.) E-mail: jeanmarie.basset@kaust.edu.sa.

Notes

The authors declare no competing financial interest.

†This work was presented at the 248th National Meeting of the American Chemical Society in San Francisco, CA, USA, August 12, 2014.

■ ACKNOWLEDGMENTS

This work was supported by funds from King Abdullah University of Science and Technology (KAUST).

■ REFERENCES

(1) Sheldon, R. A. *Chem. Soc. Rev.* **2012**, *41*, 1437−1451.

(2) Guo, Z.; Liu, B.; Zhang, Q. H.; Deng, W. P.; Wang, Y.; Yang, Y. H. *Chem. Soc. Rev.* **2014**, *43*, 3480−3524.

(3) Li, D. H. W.; Yang, L.; Lam, J. C. *Energy* **2013**, *54*, 1−10.

(4) Bravo-Suarez, J. J.; Chaudhari, R. V.; Subramaniam, B. *ACS Symp. Ser.* **2013**, *No. 1132*, 3−68.

(5) (a) Scott, S.; Basset, J.-M.; Niccolal, G.; Santini, C.; Candy, J.-P.; Lecuyer, C.; Quignard, F.; Choplin, A. *New J. Chem.* **1994**, *18*, 115−122. (b) Copéret, C.; Chabanas, M.; Saint-Arroman, R. P.; Basset, J.-M. *Angew. Chem., Int. Ed.* **2003**, *42*, 156−181.

(6) (a) Basset, J.-M., Psaro, R., Roberto, D., Ugo, R., Eds. *Modern Surface Organometallic Chemistry*; Wiley-VCH: Weinheim, Germany, 2009. (b) Copéret, C. *Chem. Rev.* **2010**, *110*, 656−680. (c) Wegener, S. L.; Marks, T. J.; Stair, P. C. *Acc. Chem. Res.* **2012**, *45*, 206−214. (d) Valla, M.; Conley, M. P.; Copéret, C. *Catal. Sci. Technol.* **2015**, DOI: 10.1039/C4CY01710B.

(7) Dufaud, V.; Basset, J.-M. *Angew. Chem., Int. Ed.* **1998**, *37*, 806−810.

(8) (a) Vidal, V.; Theolier, A.; Thivolle-Cazat, J.; Basset, J.-M. *Science* **1997**, *276*, 99−102. (b) Lefort, L.; Copéret, C.; Taoufik, M.; Thivolle-Cazat, J.; Basset, J.-M. *Chem. Commun. (Cambridge, U.K.)* **2000**, *8*, 663−664.

(9) Larabi, C.; Merle, N.; Norsic, S.; Taoufik, M.; Baudouin, A.; Lucas, C.; Thivolle-Cazat, J.; De Mallmann, A.; Basset, J.-M. *Organometallics* **2009**, *28*, 5647−5655.

(10) Rataboul, F.; Baudouin, A.; Thieuleux, C.; Veyre, L.; Copéret, C.; Thivolle-Cazat, J.; Basset, J.-M.; Lesage, A.; Emsley, L. *J. Am. Chem. Soc.* **2004**, *126*, 12541−12550.

(11) Tosin, G.; Santini, C. C.; Baudouin, A.; De Mallman, A.; Fiddy, S.; Dablemont, C.; Basset, J.-M. *Organometallics* **2007**, *26*, 4118−4127.

(12) Vidal, V.; Theolier, A.; Thivolle-Cazat, J.; Basset, J.-M.; Corker, J. *J. Am. Chem. Soc.* **1996**, *118*, 4595−4602.

(13) Le Roux, E.; Taoufik, M.; Copéret, C.; De Mallmann, A.; Thivolle-Cazat, J.; Basset, J.-M.; Maunders, B. M.; Sunley, G. J. *Angew. Chem., Int. Ed.* **2005**, *44*, 6755−6758.

(14) Chen, Y.; Abou-Hamad, E.; Hamieh, A.; Hamzaoui, B.; Emsley, L.; Basset, J.-M. *J. Am. Chem. Soc.* **2015**, *137*, 588−591.

(15) D'Ornelas, L.; Choplin, A.; Basset, J.-M.; Puga, J.; Sanchez-Delgado, R. A. *Inorg. Chem.* **1986**, *25*, 4315−4316.

(16) Samantaray, M.; Callens, E.; Abou-hamad, E.; Rossini, A.; Widdifield, C.; Dey, R.; Emsley, L.; Basset, J.-M. *J. Am. Chem. Soc.* **2014**, *136*, 1054−1061.

(17) Chen, Y.; Callens, E.; Abou-Hamad, E.; Merle, N.; White, A. J. P.; Taoufik, M.; Copéret, C.; Le Roux, E.; Basset, J.-M. *Angew. Chem., Int. Ed.* **2012**, *51*, 11886−11889.

(18) Chen, Y.; Callens, E.; Abou-hamad, E.; Basset, J.-M. *J. Organomet. Chem.* **2013**, *744*, 3−6.

(19) Chen, Y.; Ould-Chikh, S.; Callens, E.; Abou-Hamad, E.; Mohandas, J. C.; Khalid, S.; Basset, J.-M. *Organometallics* **2014**, *33*, 1205−1211.

(20) (a) Bouhoute, Y.; Garron, A.; Grekov, D.; Merle, N.; Szeto, K. C.; De Mallmann, A.; Del Rosal, I.; Maron, L.; Girard, G.; Gauvin, R. M.; Delevoye, L.; Taoufik, M. *ACS Catal.* **2014**, *4*, 4232−4241. (b) This work was presented at the ACS meeting in San Francisco, CA, USA, Aug 12, 2014: Hamieh, A.; Chen, Y.; AbouHamad, E.; Goh, S.; Emsley, L.; Basset, J.-M. In *New Well Defined Silica-Supported Tungsten Oxo Methyl Synthesized by Surface Alkylation: Application in Olefin and Paraffin Metathesis*; American Chemical Society: Washington, DC, USA, Aug 10−14, 2014; CATL-175.

(21) Blanc, F.; Basset, J.-M.; Copéret, C.; Sinha, A.; Tonzetich, Z. J.; Schrock, R. R.; Solans-Monfort, X.; Clot, E.; Eisenstein, O.; Lesage, A.; Emsley, L. *J. Am. Chem. Soc.* **2008**, *130*, 5886−5900.

(22) Weissermel, K.; Harpe, H. J. *Industrial Organic Chemistry*, 3rd ed.; VCH: Weinheim, Germany, 1997.

(23) Riache, N.; Callens, E.; Samantaray, M. K.; Kharbatia, N. M.; Atiqullah, M.; Basset, J.-M. *Chem.−Eur. J.* **2014**, *20*, 15089−15094.

(24) Siracusa, V.; Rocculi, P.; Romani, S.; Dalla Rosa, M. *Trends Food Sci. Technol.* **2008**, *19*, 634−643.

(25) Tullo, A. H. *Chem. Eng. News* **2003**, *81*, 15−16.

(26) Zhu, X. L.; Jiang, S.; Li, C. Y.; Chen, X. B.; Yang, C. H. *Ind. Eng. Chem. Res.* **2013**, *52*, 14366−14375.

DOI: 10.1021/cs5020749
ACS Catal. 2015, 5, 2164−2171

(27) Taoufik, M.; Le Roux, E.; Thivolle-Cazat, J.; Basset, J.-M. *Angew. Chem., Int. Ed.* **2007**, *46*, 7202−7205.
(28) Te Velde, G.; Bickelhaupt, F. M.; Baerends, E. J.; Guerra, C. F.; Van Gisbergen, S. J. A.; Snijders, J. G.; Ziegler, T. *J. Comput. Chem.* **2001**, *22*, 931−967.
(29) Perdew, J. P.; Burke, K.; Ernzerhof, M. *Phys. Rev. Lett.* **1997**, *78*, 1396−1396.
(30) Perdew, J. P.; Burke, K.; Ernzerhof, M. *Phys. Rev. Lett.* **1996**, *77*, 3865−3868.
(31) Feller, D. *J. Comput. Chem.* **1996**, *17*, 1571−1586.
(32) Schuchardt, K. L.; Didier, B. T.; Elsethagen, T.; Sun, L. S.; Gurumoorthi, V.; Chase, J.; Li, J.; Windus, T. L. *J. Chem. Inf. Model.* **2007**, *47*, 1045−1052.
(33) VanLenthe, E.; Ehlers, A.; Baerends, E. J. *J. Chem. Phys.* **1999**, *110*, 8943−8953.
(34) Vanlenthe, E.; Baerends, E. J.; Snijders, J. G. *J. Chem. Phys.* **1993**, *99*, 4597−4610.
(35) Vanleeuwen, R.; Vanlenthe, E.; Baerends, E. J.; Snijders, J. G. *J. Chem. Phys.* **1994**, *101*, 1272−1281.
(36) VanLenthe, E.; Snijders, J. G.; Baerends, E. J. *J. Chem. Phys.* **1996**, *105*, 6505−6516.

DOI: 10.1021/cs5020749
ACS Catal. 2015, 5, 2164−2171